Fuel 231 (2018) 352–360

Contents lists available at ScienceDirect

Fuel

journal homepage: www.elsevier.com/locate/fuel

Full Length Article

Three stages of methane adsorption capacity affected by moisture content

Kunkun Fan[a,b,*], Yajun Li[a], Derek Elsworth[b], Mingzhe Dong[a,c], Congbin Yin[d], Yanchao Li[d], Zhili Chen[a]

[a] College of Petroleum Engineering, China University of Petroleum, Qingdao 266555, China
[b] Energy and Mineral Engineering & Geosciences, G3 Center and EMS Energy Institute, Pennsylvania State University, University Park, PA 16802, USA
[c] Department of Chemical and Petroleum Engineering, University of Calgary, Calgary, AB T2N 1N4, Canada
[d] Downhole Service Company, Chuanqing Drilling Company, CNPC, Chengdu 610051, China

ARTICLE INFO

Keywords:
Shale gas
Methane adsorption capacity
Moisture content threshold
Bi-Langmuir model

ABSTRACT

Methane adsorption capacity is a key factor in determining shale gas in place (GIP) – requiring that it is determined under in situ moisture conditions. Current methods may be insufficient to investigate these exact characteristics when applied to actual reservoirs with high or variable moisture contents. We propose a heating and cooling (HC) method to prepare shale samples to arbitrary moisture contents (M_c up to 10%). A series of CH_4 adsorption experiments on two different types of shale are conducted as a function of M_c at 35 °C, 45 °C, and 55 °C, and at a CH_4 pressure of up to 10 MPa. Experimental results indicate that the methane sorption capacity versus moisture content curves exhibit a linear decreasing stage, a flat stage and a convex decreasing stage, separated by two threshold moisture contents. The lower moisture content threshold (M_{fc}) represents coverage of the entire hydrophilic surface by a monolayer of water. The upper moisture content threshold (M_{sc}) is the point at which no methane is adsorbed on the surface of the clay pores and adsorption capacity is further reduced as moisture content is increased. The linear stage with M_c up to the M_{fc} is mainly dominated by the competition between water and methane for adsorption sites on the surface of clay pores. Slope value of this stage are affected by pressure, temperature and shale compositions. The flat stage represents that the moisture content has negligible effect on shale adsorption capacity for M_c in the range M_{fc} to M_{sc}. Methane adsorption capacity decreases in a convex manner above M_{sc}, suggesting water condensation in organic pores as the surface area for methane adsorption is reduced by water blocking. A conceptual Bi-Langmuir model is presented to represent the crucial effects of moisture content on methane adsorption capacity including accurate estimations of original GIP under different reservoir conditions.

1. Introduction

Shale gas is one of the most promising unconventional natural gas resources for meeting the world's increasing energy demand [1–4]. Gas production from a particular shale play is mainly dependent on the amount of gas in place (GIP) [5–9]. However, unlike conventional gas reservoirs, gas stored in shale gas reservoirs is presumed to exist in three forms [10–14]: 1) compressed gas in the pores and fractures, 2) adsorbed gas on the surface of organic matter and clay minerals, and 3) dissolved gas in kerogen. Most of the gas stored in these different modes is in adsorbed form, due to the large internal surface area provided by the nanoscale pores in shale [15–17]. Therefore, understanding gas adsorption properties is important for an accurate evaluation of shale-gas resources and design of effective production strategies.

Shale gas adsorption capacity is a complex function of properties of shale petrophysical properties and reservoir conditions. Many researchers have recently studied shale gas adsorption characteristics and their influencing factors. There is a general agreement that the gas adsorption capacity increases with an increase in pressure and decrease in temperature [18–21]. Kerogen and clay minerals contribute the most to the total sorption isotherm [22–25]. Particle size exerts negligible influence on the amount of gas adsorbed, but has a significant effect on the dynamic adsorption process [26]. Pore deformation caused by gas adsorption and confining pressure has significant influence on gas adsorption capacity when evaluated at high pressure [27–29]. In the studies above, sorption measurements are frequently conducted on dry shale. Moisture is naturally present in certain shale reservoirs [30–32] and will inevitably be imbibed into the shale matrix during hydraulic fracturing operations [33–35], potentially exerting a profound influence on gas adsorption characteristics. Therefore, it is important to evaluate the gas sorption capacity of moist shales, to appraise the ultimate GIP more accurately. However, the exact controls and

* Corresponding author at: College of Petroleum Engineering, China University of Petroleum, Qingdao 266555, China.
E-mail address: fankunkun06@qq.com (K. Fan).

https://doi.org/10.1016/j.fuel.2018.05.120
Received 13 March 2018; Received in revised form 22 May 2018; Accepted 24 May 2018

Nomenclature

n_{ad}	number of adsorbed methane molecules, dimensionless
i	step number, dimensionless
n_t	number of total methane molecules in experimental system, dimensionless
n_{ef}	number of free methane molecules in experimental system, dimensionless
V_1	volume of standard chamber, cm^3
V_2	volume of sample chamber, cm^3
P	pressure, MPa
T	experimental temperature, K
N	step number of gas injection, dimensionless
$P_{1,N}$	standard chamber pressure corresponding to the Nth successive injection step, MPa
$P_{2,N}$	equilibrating system pressure corresponding to the Nth injection step, MPa
$Z_{1,N}$	gas compressibility factor at pressure $P_{1,N}$, dimensionless
$Z_{2,N}$	gas compressibility factor at pressure $P_{2,N}$, dimensionless
R	universal gas constant, equals to 8.314 J/(mol·K)
$P_{m2,N-1}$	steam partial equilibrating pressure at pressure $P_{2,N-1}$, MPa
$P_{m2,N}$	steam partial equilibrating pressure at pressure $P_{2,N}$, MPa
P_s	saturated vapor pressure, MPa
M_{H_2O}	molar weight of water, g/mol
ρ_{H_2O}	water density, g/cm^3
W_c	methane sorption capacity, mL/g
P_{sc}	standard atmospheric pressure, MPa
T_{sc}	temperature under standard conditions, K
M_s	sample mass, g
k	absolute slope value of the first stage of Fig. 3, dimensionless
V_{L1}, V_{L2}	Langmuir volume of clay minerals and organic matter, respectively, mL/g
P_{L1}, P_{L2}	Langmuir pressure of clay minerals and organic matter, respectively, MPa
α	water coverage coefficient on the clay surface, dimensionless
β	water filling coefficient in organic pores, dimensionless
M_c	moisture content, dimensionless
M_{fc}	lower moisture content threshold, dimensionless
M_{sc}	upper moisture content threshold, dimensionless
$r_{m,i}$	pore radius of the ith kerogen pore filled with water, nm
$V_{m,i}$	total pore volume of the ith kerogen pore filled with water, m^3/g
j	total number of pores filled with water, dimensionless
n	total number of pores in kerogen, dimensionless
r_i	pore radius of the ith pore in kerogen, nm
V_i	total pore volume of the ith pore in kerogen, m^3/g
$A_{m,i}$	surface area of the ith kerogen pore, m^2/g
γ	constant to account for water condensation in non-clay and non-kerogen pores, dimensionless
W_m	water monolayer capacity, dimensionless
TOC	total organic content, dimensionless
GIP	gas in place
HC	heating and cooling
RH	relative humidity
EW	equilibrating water

mechanisms for the effect of moisture content on shale gas adsorption behavior remains unclear.

The effect of moisture on methane adsorption capacity is investigated by comparing the adsorption capacities of moisture-equilibrated samples to those of dry samples [22,32,36,37]. The results indicate that moisture has a negative effect on the methane sorption capacity. There are two reasons accounting for this phenomenon. One is that molecular water is sorbed to specific hydrophilic sites of shale, resulting in competition between water and gas for adsorption sites. The other is that moisture condensation may make many adsorption sites unavailable to methane by blocking pore throats or occupying adsorption sites [12,13,38–40]. Despite considerable research addressing the significant effect of moisture, the exact nature of gas adsorption capacity measurements with respect to moisture content at different pressure and temperature conditions is still not well understood.

In recent studies, the role of moisture content on shale gas adsorption capacity has been quantitatively analyzed [32,41]. Shales exhibit a critical moisture content beyond which further moisture has negligible influence on gas sorption capacity. Similar results are apparent for gas adsorption capacity of moist coals [42–45]. In these studies, moisture-effect experiments are usually completed on moist samples prepared using an equilibrating water (EW) content method [22,32,37]. Samples are moistened using the vapor pressure of a certain saturated solution in vacuum desiccators with constant relative humidity (RH) [41,46]. A typical disadvantage of the EW method is the extended duration of the equilibration process for vapor phase transport. Besides, the values of the defined moisture contents are limited, due to the absence of molecular water adsorption or condensation occurring on the hydrophobic surface of organic pores when RH < 1 [47–49]. This hinders studies on gas adsorption of shales with higher moisture contents. However, it is necessary to investigate gas adsorption of moist shales covering a broad range of behaviors, due to the large and varied range of native moisture contents observed in situ [31,50]. Thus, new sample preparation methods are presented here to obtain moist shale samples with higher moisture contents, and to investigate how methane adsorption capacity is affected by water in both clay minerals and organic matter.

Herein, we present a simple and effective approach for moistening shale samples by heating and cooling (HC) the water in closed sample chambers at different temperatures. This enables any values of moisture content to be obtained by injecting different amounts of water into the sample chambers. In addition, the maximal value of moisture content is expanded (water condensation occurs in organic pores) and the equilibrating times can be significantly reduced. The methane sorption isotherm of shale samples prepared by the new HC method is shown to be valid through a comparison with shale samples prepared by the traditional EW method. We then investigate the effect of moisture content on the methane sorption capacity experimentally at pressures of up to 10 MPa, and temperatures of 35 °C, 45 °C, and 55 °C. Finally, the effect of moisture content on methane adsorption capacity at different pressure and temperature is discussed and a Bi-Langmuir model is established to predict shale gas adsorption capacity under different in situ moisture contents.

2. Experimental procedure

We introduce the HC method for preparing moist shale samples with different moisture contents. A stepped-temperature method is used to scale methane adsorption characteristics by accommodating partial pressures to account for variations in constituents of the gas phase at different pressures and temperatures.

2.1. Sample collection and characterization

Two shale samples collected from the Sichuan Basin of China are prepared for the experiments. X-ray diffraction analysis results indicate

that the mineralogical compositions of the shale are dominated by quartz, carbonates and clay minerals, as shown in Table 1. The TOC content for the outcrop shale and Longmaxi shale is 1.32% and 2.81%, respectively. Other minerals are feldspar, pyrite, and calcite.

2.2. Sample moistening method

The apparatus for preparing moist shale samples is shown in Fig. 1. Specific procedures for preparing moist shale samples are:

(1) Crush and screen shale samples at #10–#20 mesh and dry them at 105 °C for 3 days.
(2) Weigh a defined amount of the samples and compact the powder into a sample chamber.
(3) Measure the void volume of the sample chamber using a PVT method with helium.
(4) Vacuum the sample chamber and connect it with a measuring tube using a valve as shown in Fig. 1. Inject a certain amount of water into the measuring tube. Open the valve, allowing a certain amount of water to be imbibed into the sample chamber. Then close the valve.
(5) Place the sample chamber into a thermostat at 105 °C for 24 h, where the water in the sample chamber transforms to vapor.
(6) Place the sample chamber into a water bath at the designated temperature. The water will redistribute within the sample according to the moisture content and physical properties of the pore.

Through the above procedures, the moisture content can be accurately controlled and prepared to an arbitrary value within a maximal threshold. The maximal value of the moisture content for a certain shale sample chamber is only limited by the void volume of the sample chamber. In this study, the moisture content of the shale samples is prepared up to a threshold of 10%.

2.3. Moist shale adsorption experiments

Adsorption experiments are conducted on moist shales with different moisture contents at 35 °C, 45 °C, and 55 °C, using a constant-volume method similar to that presented elsewhere [51]. Procedures applied in this study differ from conventional measurements in that, instead of injecting gas to progress the experiments, temperature is varied in a controlled manner during the experimental sorption period. The benefit of this experimental method is that the moisture content within the system remains constant at all temperatures, avoiding small changes of moisture contents during the gas injection process that occurs with pressure variation.

2.4. Methane adsorption evaluation method

The number of methane molecules adsorbed (n_{ad}) during the ith step is calculated as the difference between the total number of methane molecules that exist in the setup (n_t) and the number of free molecules of methane (n_{ef}) occupying the void volume (standard chamber V_1 + sample chamber V_2), corresponding to (p, T) [12,36,52]

$$n_{ad} = n_t - n_{ef}, \tag{1}$$

The number of methane molecules in the experimental system (n_t) for N successive injection steps is calculated using

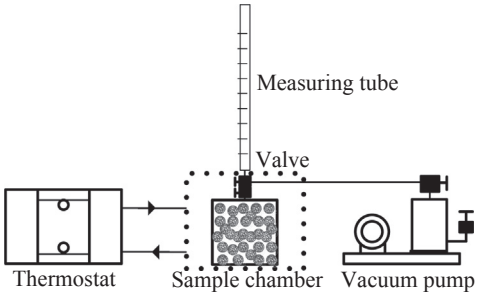

Fig. 1. Schematic diagram of the experimental apparatus for the HC method.

$$n_t = \frac{P_{1,N}V_1}{Z_{1,N}RT_1} - \frac{(P_{2,N-1} - P_{m2,N-1})V_1}{Z_{1,N-1}RT_1} + n_{t,N-1}, \tag{2}$$

In addition, the number of molecules of free methane occupying the void volume is calculated as

$$n_{ef} = \frac{(P_{2,N} - P_{m2,N})(V_1 + V_2)}{Z_{2,N}RT_1}, \tag{3}$$

where $P_{1,N}$ is the standard pressure corresponding to N of the successive injection steps (MPa); $P_{2,N}$ is the equilibrating pressure for the N injection steps (MPa); $Z_{1,N}$ and $Z_{2,N}$ are the separate gas compressibility factors at $P_{1,N}$ and $P_{2,N}$; T_1 is the temperature (K); R is the universal gas constant, 8.314 J/(mol·K) ; and $P_{m2,N-1}$ and $P_{m2,N}$ are the partial equilibrating pressures of steam separately at, $P_{2,N-1}$, $P_{2,N}$.

The partial pressure of steam is calculated as

$$ln\frac{P_{m2,N}}{P_s} = \frac{M_{H_2O}}{\rho_{H_2O}RT_1}(P_{2,N} - P_s), \tag{4}$$

where P_s is the saturated vapor pressure (MPa), M_{H_2O} is the molar weight of water (g/mol), and ρ_{H_2O} is the water density (g/cm^3).

The saturated vapor pressure corresponding to temperature T_j is calculated as [53,54]

$$log_{10}P_s = 26.209 - \frac{2960.960}{T_j} - 5.165log_{10}T_j. \tag{5}$$

The number of methane molecules adsorbed (n_{ad}) at temperature T_j is calculated by substituting Eqs. (2) and (3) into Eq. (1). The excess sorption amount at temperatureT_{j+1} when changed from T_j, is calculated from Eq. (1) by changing the temperature in Eq. (5) and corresponding parameters in Eqs. (2), (3) and (4).

The methane sorption capacity can be calculated as

$$W_c = \frac{n_{ad}RT_{sc}}{P_{sc}M_s}, \tag{6}$$

where W_w is the methane sorption capacity (mL/g), P_{sc} is the standard atmospheric pressure (MPa), T_{sc} is the temperature under standard conditions (K), and M_s is the sample mass (g).

3. Results and discussion

This section confirms the validation of the HC method and investigates the effect of the moisture content on shale adsorption capacity. Two threshold moisture contents are defined and the effects of pressure and temperature on the shale adsorption characteristics are discussed. A Bi-Langmuir model is presented to predict the methane

Table 1
TOC data and mineralogical compositions of Outcrop shale 1 and Longmaxi shale 2 samples.

Sample	Quartz (%)	Carbonates (%)	Clay minerals (%)	TOC (%)	Other minerals (%)	Vitrinite reflectance (%)
Outcrop shale 1	36.89	31.38	8.8	1.32	14.22	1.69
Longmaxi shale 2	30.53	31.35	18.28	2.81	14.36	2.67

adsorption capacity of shale with different moisture contents.

3.1. Validation of the HC method

To validate the HC method, both the HC and EW methods are used to prepare moist shale samples for evaluation of methane sorption capacities. Fig. 2 shows methane sorption isotherms of shale Sample #1 with two moisture contents at a temperature of 35 °C. The methane sorption capacity of the samples, saturated using the two moisture methods, is almost identical at a moisture content level of 3%, and only slightly different at a moisture content level of 0.5%. The relative error in the methane capacity between the two moistened samples with a moisture content level of 0.5% is within 5%. This is within an acceptable range. Thus, it is reasonable to study the methane sorption isotherm of moist shale saturated using the HC method.

Compared with the EW method, the HC method has several advantages. First, the maximal value of the moisture content obtained from the HC method is larger than that from the EW method. Besides, shale samples with an arbitrary moisture content level can be easily prepared using the HC method, compared to the much more difficult and complex EW method. Another advantage for the HC method is in saving time.

In the EW method, the RH remains constant when preparing moist shale at each moisture content. However, in the HC method, RH is variable with moisture distribution over pressures in the range from 105 °C to the designated temperature. This may result in enigmatic water distribution characteristics in both organic and inorganic pores of the shale [48,55]. and complex mechanisms of methane adsorption at different moistures content levels. Fortunately, Fig. 2 shows that moist shale samples examined by both HC and EW methods possess identical adsorption capacities at the same moisture content levels. Therefore, it is acceptable to use an assumption that the water distribution characteristics in the HC method is equivalent to that in the EW method when the moisture content level is less than the value obtained from EW method at RH = 97%. Experimental results indicate that the moisture contents at RH = 97% are approximately 3.0% and 3.5% for Sample #1 and Sample #2, respectively. Using this assumption, the effect of moisture content on adsorption capacity in shale will be discussed in detail in later section.

3.2. Effects of moisture content on methane adsorption

To study the effects of moisture content on methane adsorption in detail, the amount of methane adsorption on shale samples at 2, 4, 6, 8, and 10 MPa is calculated by fitting methane adsorption isotherms at different temperatures and moisture contents. The relationship between the maximum methane adsorption capacity and moisture content can be calculated, as shown in Fig. 3.

Fig. 3 shows that the methane maximum adsorption capacity has a stepped variation with the moisture content (M_c) at certain pressure and temperature conditions, which can be divided into three stages by two threshold moisture contents: (i) In the region from dry conditions to moisture content approaching the lower moisture content threshold, M_{fc}, the methane adsorption capacity decreases linearly with an increase in M_c. (ii) In the region in which M_c ranges from M_{fc} to the upper moisture content threshold, M_{sc}, methane adsorption capacity remains almost constant with an increase in M_c. (iii) In the region in which M_c ranges from M_{sc} to 10%, the methane adsorption capacity further reduces with a convex shape.

During the first stage in Fig. 3, water molecules attach to the hydrophilic surface of clay pores, and the methane adsorption capacity reduces with the increase in M_c. The methane adsorption sites are occupied by a monolayer of water [44,48,55–57] in this stage. Hence, the methane adsorption capacity decreases linearly with an increase in M_c, until an entire hydrophilic surface is occupied by a monolayer of water. The point at which the entire hydrophilic surface is occupied by monolayer water corresponds to the lower threshold (M_{fc}) [44], as shown in Fig. 4(a). This means that the value of the water monolayer capacity (W_m) is equal to the value of M_{fc}. Because water only attaches to the hydrophilic surface of the clay pores in this stage, the hydrophobic surface of organic pores remains available for the adsorption of methane. Sample #2 contains a higher proportion of clay minerals, and its water surface areas are higher than those of Sample #1. Therefore, the W_{fc} of Sample #2 is larger than that of Sample #1 at the same pressure and temperature.

The second stage in Fig. 3 shows a negligible decrease in methane sorption with an increase in moisture uptake. When M_{fc} is exceeded, multilayer adsorption of water molecules occurs on the surface of the clay minerals, as shown in Fig. 4(b). The adsorbed water molecules further occupy space that would be available to methane when M_c is at the monolayer capacity. The number of the occupied hydrophobic sites is small. Thus, the decrease in methane adsorption capacity is negligible with M_c up to the upper moisture content threshold, M_{sc}.

The M_{sc} is the point at which no methane is adsorbed on the surface of the clay minerals and adsorption capacity will reduce when moisture content is increased. In other words, at the M_{sc}, condensate water fills the pores of the clay minerals and only adsorption sites on the surface of organic matter are available to methane. This is consistent with the greater proportional effect of clay content on the methane sorption capacity at the M_{sc}. Compared with dry conditions, for Sample #1, the reduction in methane capacity is ~35%, but for Sample #2, the capacity is reduced by more than 45% at the M_{sc} within the range of our experiment conditions.

When the moisture content is above the M_{sc}, water condensation may occur in the pores of the organic matter. The processes of water condensation in organic and inorganic pores differ. According to a previous study [47], there exists an equilibrium thickness for the film of uniform thickness with which the bulk liquid (for organic and inorganic pores) is at equilibrium. When the thickness of a water film is larger than when at equilibrium, the water film will jump to form a liquid plug occupying the entire surface area of the inner pores. However, the equilibrium of the thickness of the wetting film on an organic pore surface is less than for the thickness of a monolayer, which means that only water molecules exist in the organic pores before the water condensation. In other words, no liquid film forms initially on the surface of the organic matter. As the moisture content increases, water condensation will jump to form a liquid plug occupying the entire space of some organic pores, as shown in Fig. 4(c).

Water condensation at RH < 1 only occurs in the organic pores with diameter less than 1 nm, and condensation in large pores occurs at RH > 1 [47]. In this study, the moist shale samples are prepared using the HC method, where the samples rest at a high temperature at 105 °C

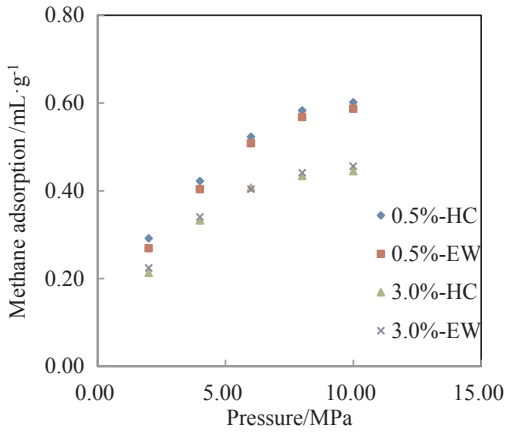

Fig. 2. Methane sorption isotherms at different moisture content levels of Sample #1 moistened using a heating and cooling (HC) method and an equilibrating water (EW) method.

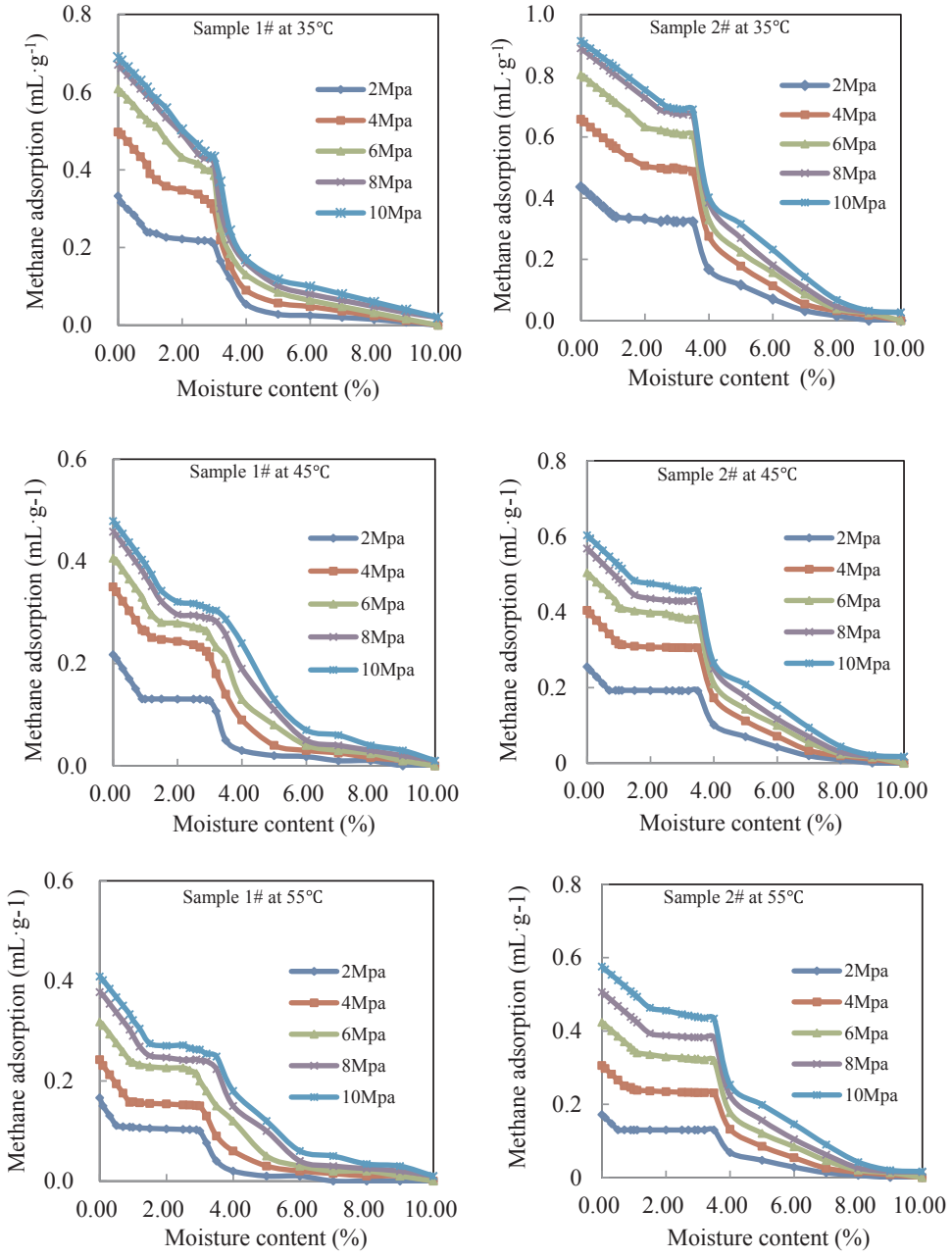

Fig. 3. Effects of M_c on methane maximum sorption capacity for two shale samples at different pressure and temperature levels.

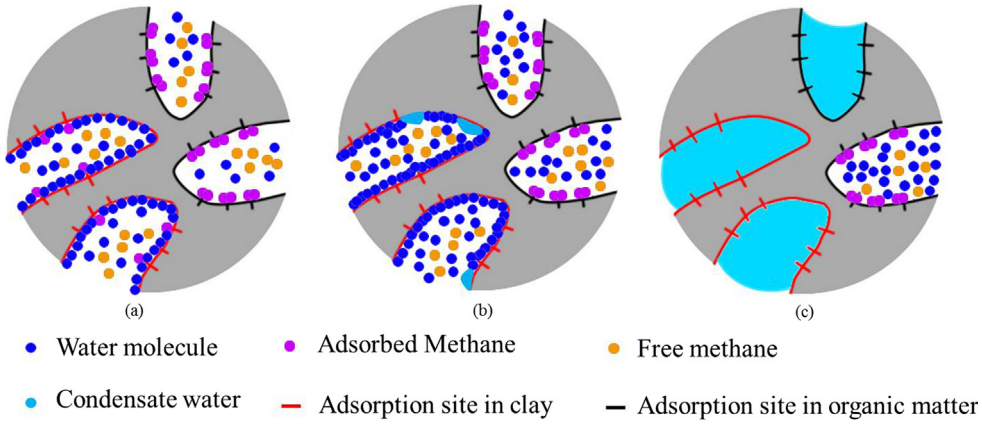

Fig. 4. Schematic representation of methane and moisture adsorption in shale pores with an increase in the moisture content: (a) monolayer adsorption of molecular water [44,48,55–57] on the surface of clay pores with methane adsorption on the surface of clay and organic pores (not otherwise occupied by molecular water), (b) multilayer water adsorption and partial condensation of water on the surface of the clay pores with negligible methane adsorption on the surface of the clay pores and (c) condensed water throughout the clay pores and in some organic pores with methane adsorption only occurring in some of the organic pores.

for 24 h, providing a condition of RH > 1. As discussed before, if M_c is less than the M_{sc}, water will preferentially adsorb and condense in the pore interiors of clay minerals. When M_c is exceeded the M_{sc}, water condensation will occur in the organic pores. Thus, the adsorption sites in the organic matter are inevitably occupied by condensed water. This will further reduce the methane adsorption capacity, as shown in Fig. 3. If moisture content is sufficiently high to occupy all pores of the shale, no methane will be adsorbed. The third stage in Fig. 3 can be described using a parabolic segment, whose shape differs from that in the first stage in the figures. This difference is cause by the phenomenon in which water condenses progressively in organic pores with different pore sizes.

3.3. Effects of temperature and pressure on methane adsorption

The negative effect of temperature and the positive effect of pressure on methane sorption in dry shale samples have been widely recognized [12,13,19,51,58]. However, no systematic description of the effects of pressure and temperature on gas adsorption capacity of moist shale is available, leading to a lack of basic data and understanding of mechanisms. To acquire a basic knowledge for evaluating the GIP of shale under real reservoirs conditions, the effects of pressure and temperature on methane adsorption characteristics of moist shale are discussed in detail in this section.

3.3.1. M_c-sorption gradients in the linear stage

We use a value of k representing the slope of the linear stage in Fig. 3. The larger the value of k, the greater the rate of sorption change relative to M_c. Fig. 5 shows the effects of temperature and pressure on the value of k.

As Fig. 5 indicates, the value of k decreases with an increase in pressure, and the rate of decrease is greater at low pressure than at high pressure. This phenomenon can be explained using previous molecular simulation results [59], which expresses the potential methane energy distribution curve under different moisture contents. It can be concluded from the molecular simulation results that the energy distribution curve between methane and clay pore surfaces has two peaks, the main one of which lies in an area of higher energy, and the secondary one is located in an energy well. Only the secondary peak of the potential energy distribution curve gradually becomes gentler as the water content increases, indicating that the methane molecules in the higher energy adsorption sites do not move with the change in moisture content. It can be determined that the molecular water mainly occupies the lower energy adsorption sites on the clay pore walls instead of the higher energy adsorption sites, illustrating that the water and methane compete for adsorption space on a lower energy adsorption site. At lower pressure, most of the methane molecules adsorb onto lower energy adsorption sites, and a small amount of methane molecules adsorb onto higher energy adsorption sites. At higher pressure, the methane molecules can adsorb onto both lower and higher energy adsorption sites. Hence, the water molecules have a greater effect on the methane adsorption capacity at lower pressure than at higher pressure, which leads to a decrease in the value of k as the pressure increases.

When the temperature increases, both methane and water move to adsorb onto lower energy adsorption sites. Therefore, a different approach should be used to describe the effects of temperature on the value of k. At the same pressure, the partial pressure of water vapor at higher temperature is larger than that at lower temperature, which leads to a smaller number of adsorption sites occupied by water molecules at higher temperature than at lower temperature. Thus, the water molecules have a greater effect on the methane adsorption capacity at lower temperature than at higher temperature. This is an explanation for the negative effect of temperature on value of k.

Fig. 5 also indicates that the value of k for different samples shows a similar mode of response. Clay minerals are the key factor impacting the methane adsorption capacity of shale because of water molecules adsorbed on the surface of the clay pores. Organic pores are not affected by water molecules at this stage. Therefore, an increase in organic matter will decrease the value of k. The content of organic matter in Sample # 2 is higher than that in Sample # 1, and the value of k for Sample # 2 is smaller than that for Sample # 1 at the same conditions.

3.3.2. Threshold moisture contents

In the sorption tests, moisture content is applied in a sample chamber under a series of particular values before the sample chamber is connected to the standard chamber. Two problems may occur in the determination of the proper threshold moisture contents. First, the actual critical moisture content may not be the value used for the moist samples. We should use the intersection points of the extended curves at different stages in Fig. 3 to determine the two threshold moisture contents. In addition, a loss of water may occur in the sample chamber when connected with the standard chamber. We should use Eqs. (4) and (5) to correct the moisture content in the sample chamber. Experiment results show that the lower threshold is affected by the pressure and temperature. However, the upper threshold is only affected by the shale composition and changes little with the pressure and temperature. The upper threshold is 3% and 3.5% for samples #1 and #2, respectively-the value is equal to moisture contents of shale saturated at RH = 97%. Therefore, the upper threshold can be determined from the moisture isotherm of the shale. Effects of pressure and temperature on the lower threshold are shown in Fig. 6. It can be seen that the lower threshold of those two samples increases with an increase in pressure and decrease in temperature.

Both the pressure and temperature affect the lower threshold by affecting the adsorption sites on the pore surface and the partial vapor pressure in the void space. At the M_{fc}, the number of adsorption sites for water adsorption remains nearly unchanged as the pressure increases, according to the potential energy distribution curves [59], whereas the partial vapor pressure increases with a pressure increase. Therefore, the M_{fc} increases with the increase in pressure.

When the temperature increases, the number of adsorption sites for water adsorption decreases, contributing to a smaller value of the M_{fc}. In contrast, the partial vapor pressure increases with an increase in temperature, thereby leading to a greater value of the M_{fc}. Fig. 6 shows that the M_{fc} decreases with an increase in temperature, indicating that the M_{fc} is much more sensitive to the decrease of the number of adsorption sites than to the increase of partial vapor pressure as the temperature increases.

3.4. Model for predicting methane adsorption capacity

3.4.1. Model

This section presents a Bi-Langmuir model to predict shale methane

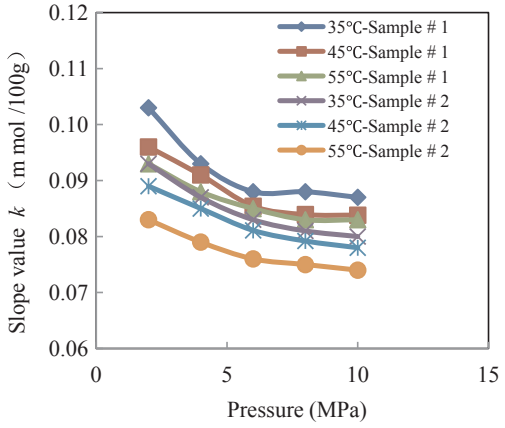

Fig. 5. Relationship between slope value k of the decrease in methane sorption capacity and pressure at different temperatures for two samples.

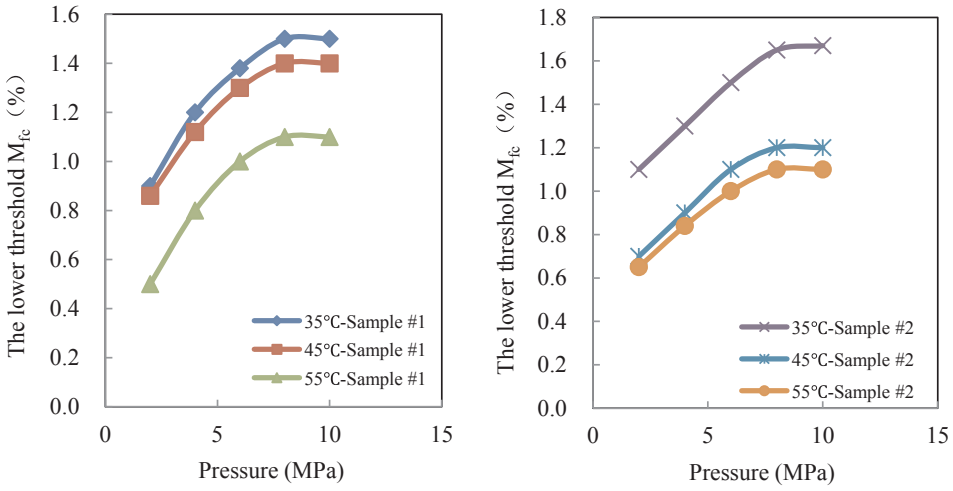

Fig. 6. Relationship between the lower threshold and pressure at different temperatures for two samples.

adsorption capacity at different moisture contents by considering the methane adsorption capacity as a sum of individual sorption capacities of both clay minerals and organic matter. In order to simplify the mathematical analysis, we assume that both water and methane are adsorbed on the inner surface of the shale pores of cylindrical geometry [60–62]. The Bi-Langmuir model is based on the usual monolayer adsorption of methane and multi-layer adsorption of molecular water [22,48]. The adsorption capacity of the moist shale can be represented as a sum of adsorption isotherms of the clay minerals and organic matter [11], as:

$$W_c = (1-\alpha)\frac{V_{L1}P}{P_{L1}+P} + (1-\beta)\frac{V_{L2}P}{P_{L2}+P} \quad (7)$$

where V_{L1} and V_{L2} are the Langmuir volumes of clay minerals and organic matter, respectively (mL/g), P_{L1} and P_{L2} are the Langmuir pressures of clay minerals and organic matter, respectively (MPa), α is water coverage coefficient on the clay surface (dimensionless), and β is a water filling coefficient in the organic pores (dimensionless), with α and β, both in the range 0–1.

3.4.2. Methane adsorption capacity determination

In order to determine methane adsorption capacity at different moisture contents, each unknown parameter in Eq. (7) may be evaluated as follows:

(1) Conduct methane adsorption experiments on moist shale with two different moisture contents in both the first and second stages of Fig. 3, respectively. Determine an accurate M_{fc} by calculating the intersection of the two stage lines.
(2) Determine the M_{sc} by measuring the value of the moist shale isotherm corresponding to RH = 0.97.
(3) Determine the parameters (V_{L1}, $P_{L1}V_{L2}$, P_{L2}) of the Bi-Langmuir model of Eq. (7) with $\alpha = \beta = 1$, by fitting the methane adsorption isotherm of the dry shale.
(4) Calculateα and β at different moisture contents. When M_c is less than M_{fc}, $\alpha = M_c/Mfc'$, and $\beta = 0$ with $\alpha = 1$ and $\beta = 0$ for M_c in the range from M_{fc} to M_{sc}. When is M_c larger than M_{sc}, $\alpha = 1$ and the values of β can be determined with the assumption of cylindrical pores, and written as:

$$\beta = \frac{\sum_{i}^{j} V_{m,i}/r_{m,i}}{\sum_{i}^{n} V_i/r_i} \quad (8)$$

where and $V_{m,i}$ are the pore radius and total pore volume of the ith kerogen pore filled with water ((nm) and (m^3/g), respectively). j is the total number of pores filled with water. n is the total number of pores in kerogen, and r_i and V_i are pore radius and total pore volume of the i^{th} pore in kerogen.

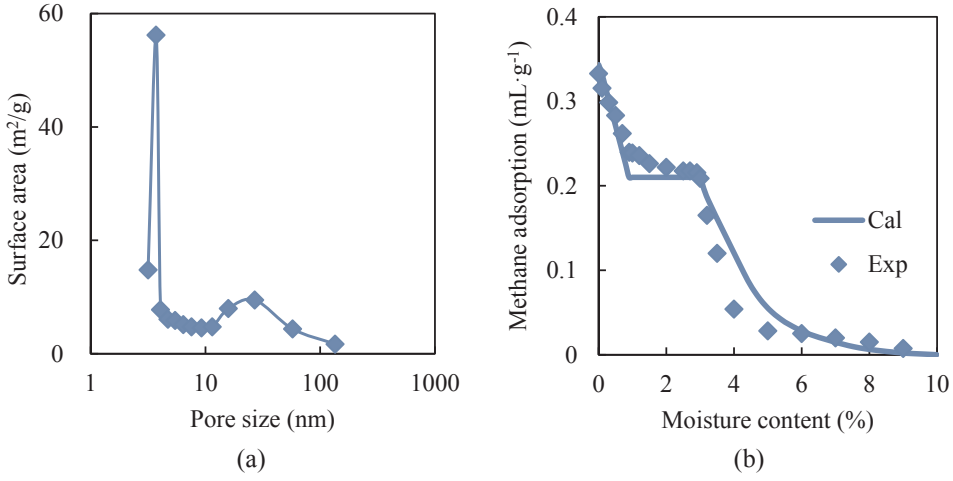

Fig. 7. A case verifying the Bi-Langmuir model with (a) Pore size distributions of kerogen in Lomgmaxi shale and (b) calculated and experimental methane adsorption capacity vs. moisture content.

Since water condensation occurs from small pores to large pores, the value of j can be determined from:

$$\gamma \sum_{i}^{j} V_{m,i} = \gamma \sum_{i}^{j} \frac{A_{m,i} r_i}{2} = \frac{M_c - M_{sc}}{\rho_{H_2O}} \tag{9}$$

where $A_{m,i}$ is surface area of the ith kerogen pore, (m^2/g), and γ is a constant to account for water condensation in other non-clay and non-kerogen pores – γ = 15.38 in this study.

Therefore, combining Eqs. (7), (8) and (9), the model to determine methane adsorption content under different water contents can be given by:

$$W_c = \left(1 - \frac{M_c}{M_{fc}}\right) \frac{V_{L1} P}{P_{L1} + P} + \frac{V_{L2} P}{P_{L2} + P}, \quad 0 \leqslant M_c < M_{fc} \tag{10-1}$$

$$W_c = \frac{V_{L2} P}{P_{L2} + P}, \quad M_{fc} \leqslant M_c \leqslant M_{sc} \tag{10-2}$$

$$W_c = \left(1 - \frac{\sum_{i}^{j} A_{m,i}}{\sum_{i}^{n} A_i}\right) \frac{V_{L2} P}{P_{L2} + P}, \quad M_{sc} \leqslant M_c \tag{10-3}$$

3.4.3. Model verification and applicability analysis

Note that the determination of methane capacity (when $M_c \geqslant M_{sc}$) is based on the pore size distribution within the kerogen. In this study, we take a typical kerogen pore size distribution as an example to predict methane adsorption capacity of moist shale, as shown in Fig. 7(a) [63]. The pore diameter ranges from 3.2 to 135 nm, with a major peak at ~3.7 nm.

The experimental and calculated relationship between the methane absorption and moisture content for Sample #1 at a pressure of 2 MPa and temperature 35 °C are shown in Fig. 7(b) – identifying the congruence between calculated and experimental results. This indicates that this analysis gives a reasonable description of mechanisms of the effect of moisture content on methane adsorption capacity of the shale. However, the model presented in this study is only a lumped-parameter model and the process of water distribution on the surface of inorganic and organic pores is not discussed. Besides, methane sorbed as water-monolayers on the surface of the shale is neglected. However, overall, this study reveals some basic mechanisms for the change in shale adsorption capacity with moisture content. This is of great importance for GIP evaluation and prediction in shale gas reservoirs.

4. Conclusions

In this study, laboratory experiments are conducted to investigate the effects of moisture content on adsorption capacity of shale. A conceptual Bi-Langmuir model is presented to predict methane absorption capacity by accommodating the effect of moisture content. Major conclusions of this study are as follows:

(1) A new HC method is confirmed to be valid for preparing moist shale samples with different moisture contents.
(2) The relationship between methane adsorption capacity and moisture content is revealed to be in three stages, separated by two moisture content thresholds (M_{fc} and M_{sc}). Mechanisms for the effect of moisture content on methane adsorption are mainly dominated by two aspects: a) competition between water and methane for adsorption sites on the surface of clay pores when M_c is less than the lower threshold, M_{fc}; and b) condensation of water in organic pores blocking the available surface area for methane adsorption when M_c is larger than the upper threshold, M_{sc}.
(3) The absolute slope value, k, is a function of pressure, temperature and shale composition. Increases in both pressure and temperature reduce the value of k. This phenomenon can be explained by the potential energy distribution of the methane on the surface of the clay minerals. An increase in organic matter decreases the value of k, because moisture content has no effect on adsorption capacity of organic matter when M_c is less than M_{fc}.
(4) The M_{fc} of the two shale samples increases with an increase in pressure and decrease in temperature, due to the changes of the adsorption sites on the pore surface and the partial vapor pressure in the void space. The M_{sc} is little influenced by pressure and temperature, and is 3% and 3.5% for samples #1 and #2, respectively. This approximately corresponds to the equilibrium moisture content obtained from the moisture isotherm of shale at RH = 97%.
(5) A conceptual Bi-Langmuir model is successfully applied to predict methane absorption capacity under different moisture contents in shale systems, which provides a basic approach for GIP evaluation and prediction in shale gas reservoirs.

Acknowledgements

We are grateful for the important support from the 973 Project (2014CB239103), the National Science & Technology Major Project (2016ZX05023-001, 2017ZX05049-006), the Fundamental Research Funds for Central Universities (15CX06026A), the China Scholarship Council (201706450021) and the Graduate Innovation Fund Project of China University of Petroleum (Huadong) (YCXJ2016018).

Notes

The authors declare no competing financial interest.

References

[1] Guo C, Wei M, Hong L. Modeling of gas production from shale reservoirs considering multiple transport mechanisms. PLoS One 2015;10:1–14.
[2] Mcglade C, Speirs J, Sorrell S. Unconventional gas – a review of regional and global resource estimates. Energy 2013;55:571–84.
[3] Jarvie DM, Hill RJ, Ruble TE, Pollastro RM. Unconventional shale-gas systems: the Mississippian Barnett Shale of north-central Texas as one model for thermogenic shale-gas assessment. Am Assoc Pet Geol Bull 2007;91:475–99.
[4] Cao P, Liu J, Leong YK. A multiscale-multiphase simulation model for the evaluation of shale gas recovery coupled the effect of water flowback. Fuel 2017;199:191–205.
[5] Sang Q, Li Y, Yang Z, Zhu C, Yao J, Dong M. Experimental investigation of gas production processes in shale. Int J Coal Geol 2016;159:30–47.
[6] Guo C, Xu J, Wu K, Wei M, Liu S. Study on gas flow through nano pores of shale gas reservoirs. Fuel 2015;143:107–17.
[7] Shi J, Zhang L, Li Y, Yu W, He X, Liu N, et al. Diffusion and Flow Mechanisms of Shale Gas through Matrix Pores and Gas Production Forecasting. In: SPE Unconventional Resources Conference Canada, Calgary, Alberta, Canada, 5–7 November 2013.
[8] Wu K, Chen Z, Li X. Real gas transport through nanopores of varying cross-section type and shape in shale gas reservoirs. Chem Eng J 2015;281:813–25.
[9] Amann-Hildenbrand A, Ghanizadeh A, Krooss BM. Transport properties of unconventional gas systems. Mar Pet Geol 2012;31:90–9.
[10] Sandoval DR, Yan W, Michelsen ML, Stenby EH. Modeling of shale gas adsorption and its influence on phase equilibrium. Ind Eng Chem Res 2018;57:5736–47.
[11] Lu X, Li F, Watson A. Adsorption studies of natural gas storage in Devonian shales. SPE Form Eval 1995;10:109–13.
[12] Ross DJK, Bustin RM, Zhang T, Ellis GS, Ruppel SC, Milliken K, et al. Effect of organic-matter type and thermal maturity on methane adsorption in shale-gas systems. Org Geochem 2012;47:120–31.
[13] Ross DJK, Bustin RM. Shale gas potential of the Lower Jurassic Gordondale Member, northeastern British Columbia, Canada. Bull Can Pet Geol 2007;55:51–75.
[14] Culver EL, Makuch M, Vermeulen E, Van Leeuwen A, Sadler R, Cargill T, et al. Geochemical constraints on the origin and volume of gas in the New Albany Shale (Devonian–Mississippian), eastern Illinois Basin. Bookbird World Child Books 2010;94:32–4.
[15] Ma J, Couples GD. Assessing Impact of Shale Gas Adsorption on Free-Gas Permeability via a Pore Network Flow Model. In: Unconventional Resources Technology Conference, Texas, United States, 20–22 July 2015.
[16] Hill DG, Nelson CR. Gas productive fractured shales: an overview and update. Gas Tips 2000;6:4–13.
[17] Peng Y, Liu J, Pan Z, Connell LD. A sequential model of shale gas transport under the influence of fully coupled multiple processes. J Nat Gas Sci Eng 2015;27:808–21.

[18] Rexer TF, Mathia EJ, Aplin AC, Thomas KM. High-pressure methane adsorption and characterization of pores in Posidonia Shales and isolated Kerogens. Energy Fuels 2014;28:2886–901.
[19] Rexer TFT, Benham MJ, Aplin AC, Thomas KM. Methane adsorption on shale under simulated geological temperature and pressure conditions. Energy Fuels 2013;27:3099–109.
[20] Thomas L. Coal geology. John Wiley & Sons; 2002.
[21] Etminan SR, Javadpour F, Maini BB, Chen Z. Measurement of gas storage processes in shale and of the molecular diffusion coefficient in kerogen. Int J Coal Geol 2014;123:10–9.
[22] Yuan W, Pan Z, Li X, Yang Y, Zhao C, Connell LD, et al. Experimental study and modelling of methane adsorption and diffusion in shale. Fuel 2014;117:509–19.
[23] Schettler PD, Parmely CR. Contributions to Total Storage Capacity in Devonian Shales. In: SPE Eastern Regional Meeting, Lexington, Kentucky, United States, 22–25 October 1991.
[24] Wang S, Javadpour F, Feng Q. Fast mass transport of oil and supercritical carbon dioxide through organic nanopores in shale. Fuel 2016;181:741–58.
[25] Wang S, Feng Q, Javadpour F, Xia T, Li Z. Oil adsorption in shale nanopores and its effect on recoverable oil-in-place. Int J Coal Geol 2015;147–148:9–24.
[26] Wang J, Wang B, Li Y, Yang Z, Gong H, Dong M. Measurement of dynamic adsorption–diffusion process of methane in shale. Fuel 2016;172:37–48.
[27] Kang SM, Fathi E, Ambrose RJ, Akkutlu IY, Sigal RF. Carbon dioxide storage capacity of organic-rich shales. SPE J 2011:842–55.
[28] Santos JM, Akkutlu IY. Laboratory measurement of sorption isotherm under confining stress with pore-volume effects. SPE J 2013;18:924–31.
[29] Sigal RF, Akkutlu IY, Kang SM, Diaz-Campos M, Ambrose R. The laboratory measurement of the gas-storage capacity of organic shales. Petrophysics 2013;54:224–35.
[30] Jarvie DM. Shale resource systems for oil and gas: part 1—shale-gas resource systems. Shale Reserv Resour 21st Century AAPG Mem 2012;97:69–87.
[31] Jarvie DM. Shale resource systems for oil and gas: part 2—shale-oil resource systems. Shale Reserv Resour 21st Century AAPG Mem 2012;97:89–119.
[32] Merkel A, Fink R, Littke R. The role of pre-adsorbed water on methane sorption capacity of Bossier and Haynesville shales. Int J Coal Geol 2015;147–148:1–8.
[33] Dehghanpour H, Lan Q, Saeed Y, Fei H, Qi Z. Spontaneous imbibition of brine and oil in gas shales: effect of water adsorption and resulting microfractures. Energy Fuels 2013;27:3039–49.
[34] Ge HK, Yang L, Shen YH, Ren K, Meng FB, Ji WM, et al. Experimental investigation of shale imbibition capacity and the factors influencing loss of hydraulic fracturing fluids. Pet Sci 2015;12:636–50.
[35] Bennion DB, Bietz RF, Thomas FB, Cimolai MP. Reductions in the productivity of oil & gas reservoir due to aqueous phase trapping. J Can Pet Technol 1994;33.
[36] Gasparik M, Ghanizadeh A, Bertier P, Gensterblum Y, Bouw S, Krooss BM. High-pressure methane sorption isotherms of black shales from The Netherlands. Energy Fuels 2012;26:4995–5004.
[37] Tan J, Weniger P, Krooss B, Merkel A, Horsfield B, Zhang J, et al. Shale gas potential of the major marine shale formations in the Upper Yangtze Platform, South China, Part II: methane sorption capacity. Fuel 2014;129:204–18.
[38] Krooss BM, Van Bergen F, Gensterblum Y, Siemons N, Pagnier HJM, David P. High-pressure methane and carbon dioxide adsorption on dry and moisture-equilibrated Pennsylvanian coals. Int J Coal Geol 2002;51:69–92.
[39] Ross DJK, Bustin RM. Characterizing the shale gas resource potential of Devonian-Mississippian strata in the Western Canada sedimentary basin: application of an integrated formation evaluation. Am Assoc Pet Geol Bull 2008;92:87–125.
[40] Ross DJK, Marc Bustin R. The importance of shale composition and pore structure upon gas storage potential of shale gas reservoirs. Mar Pet Geol 2009;26:916–27.
[41] Branson K, Newman ACD. Water sorption on Ca-saturated clays: I. multilayer sorption and microporosity in some illites. Clay Miner 1983;18:277–87.
[42] Levy JH, Day SJ, Killingley JS. Methane capacities of Bowen Basin coals related to coal properties. Fuel 1997;76:813–9.
[43] Joubert JI, Grein CT, Bienstock D. Effect of moisture on the methane capacity of American coals. Fuel 1974;53:186–91.
[44] Day S, Sakurovs R, Weir S. Supercritical gas sorption on moist coals. Int J Coal Geol 2008;74:203–14.
[45] Joubert JI, Grein CT, Bienstock D. Sorption of methane in moist coal. Fuel 1973;52:181–5.
[46] Ewy RT. Shale/claystone response to air and liquid exposure, and implications for handling, sampling and testing. Int J Rock Mech Min Sci 2015;80:388–401.
[47] Mattia D, Starov V, Semenov S. Thickness, stability and contact angle of liquid films on and inside nanofibres, nanotubes and nanochannels. J Colloid Interface Sci 2012;384:149–56.
[48] Hatch CD, Wiese JS, Crane CC, Harris KJ, Kloss HG, Baltrusaitis J. Water adsorption on clay minerals as a function of relative humidity: application of BET and Freundlich adsorption models. Langmuir 2012;28:1790–803.
[49] Chalmers GR, Bustin RM, Power IM. Characterization of gas shale pore systems by porosimetry, pycnometry, surface area, and field emission scanning electron microscopy/transmission electron microscopy image analyses: examples from the Barnett, Woodford, Haynesville, Marcellus, and Doig uni. Am Assoc Pet Geol Bull 2012;96:1099–119.
[50] Chalmers GR, Bustin MR. The Effects and Distribution of Moisture in Gas Shale Reservoir Systems. In: AAPG Annual Convention and Exhibition, New Orleans, Louisiana, United States, 11–14 April 2010.
[51] Gasparik M, Ghanizadeh A, Gensterblum Y, Krooss BM. "Multi-temperature" method for high-pressure sorption measurements on moist shales. Rev Sci Instrum 2013;84:1–10.
[52] Ren W, Li G, Tian S, Sheng M, Geng L. Adsorption and surface diffusion of supercritical methane in shale. Ind Eng Chem Res 2017;56:3446–55.
[53] Miller DG. Estimating vapor pressures-a comparison of equations. Ind Eng Chem 1964;56:46–57.
[54] Wexler A, Greenspan L. Vapor pressure equation for water in the range 0 to 100 °C. J Res Natl Bur Stand Sect A Phys Chem 1971;75A:213–45.
[55] Li J, Li X, Wang X, Li Y, Wu K, Shi J, et al. Water distribution characteristic and effect on methane adsorption capacity in shale clay. Int J Coal Geol 2016;159:135–54.
[56] Li J, Li X, Wang X, Li Y, Wu K, Shi J, et al. Water distribution characteristic and effect on methane adsorption capacity in shale clays. In: SPE Asia Pacific Unconventional Resources Conference and Exhibition, Brisbane, Australia, 9–11 November 2015.
[57] Say KO, Lion LW. Trichloroethylene vapor sorption onto soil minerals. Soil Sci Soc Am J 1991;55:1559–68.
[58] Lu XC, Li FC, Watson AT. Adsorption measurements in Devonian shales. Fuel 1995;74:599–603.
[59] Xiong J, Liu X-J, Liang L-X, Zeng Q. Investigation of methane adsorption on chlorite by grand canonical Monte Carlo simulations. Pet Sci 2017;14:37–49.
[60] Yang Z, Wang W, Dong M, Wang J, Li Y, Gong H, et al. A model of dynamic adsorption-diffusion for modeling gas transport and storage in shale. Fuel 2016;173:115–28.
[61] Cui X, Bustin AMM, Bustin RM. Measurements of gas permeability and diffusivity of tight reservoir rocks: different approaches and their applications. Geofluids 2009;9:208–23.
[62] Fan K, Dong M, Elsworth D, Li Y, Yin C, Li Y. A dynamic-pulse pseudo-pressure method to determine shale matrix permeability at representative reservoir conditions. Int J Coal Geol 2018;193:61–72.
[63] Cao T, Song Z, Wang S, Xia J. A comparative study of the specific surface area and pore structure of different shales and their kerogens. Sci China Earth Sci 2015;58:510–22.